Quaternary International 748 (2025) 109969

Contents lists available at ScienceDirect

Quaternary International

journal homepage: www.elsevier.com/locate/quaint

Loess provenance in the westernmost part of the lower Danube Basin, Serbia: Geochemical insights from the Velika Vrbica fluvial–eolian section

Petar Krsmanović [a], Zoran M. Perić [b,*], Warren Thompson [c], Milica G. Radaković [a], Cathal S. Ryan [b], Randall J. Schaetzl [d], Qingzhen Hao [e], Tin Lukić [a], Helena Alexanderson [b], Slobodan B. Marković [f,g,h,i]

[a] Chair of Physical Geography, Department of Geography, Tourism and Hotel Management, Faculty of Sciences, University of Novi Sad, Trg Dositeja Obradovića 3, 21000, Novi Sad, Serbia
[b] Department of Geology, Lund University, Sölvegatan 12, SE-22362, Lund, Sweden
[c] Nordic Laboratory for Luminescence Dating, Risø Campus, DTU Physics, DK-4000, Roskilde, Denmark
[d] Department of Geography, Environment, and Spatial Sciences, 673 Auditorium Rd., Michigan State University, East Lansing, MI, 48823, USA
[e] Key Laboratory of Cenozoic Geology and Environment, Institute of Geology and Geophysics, Chinese Academy of Sciences, Beijing, 100029, China
[f] Division of Geochronology and Environmental Isotopes, Institute of Physics – Centre for Science and Education, Silesian University of Technology, Gliwice, Poland
[g] Serbian Academy of Sciences and Arts, Kneza Mihaila 35, 11000, Belgrade, Serbia
[h] University of Montenegro, Cetinjska 2, 81000, Podgorica, Montenegro
[i] Laboratory for Paleoecological Reconstruction (LAPER), Faculty of Sciences, University of Novi Sad, Trg Dositeja Obradovića 3, 21000 Novi Sad, Serbia

ARTICLE INFO

Keywords:
Loess
Geochemistry
OSL
Upper Pleistocene
Sediment provenance
Serbia

ABSTRACT

Our study examined the chemical composition of fluvial and eolian sediments at the Velika Vrbica multisection, located on the bank of the Danube River in eastern Serbia, within the westernmost part of the lower Danube (Dacian) Basin. The multisection comprises two discrete sections: an older 2.7 m thick fluvial section, and a younger 11.2 m thick loess-paleosol sequence (LPS). These are exposed along the sides of a gully incised into a Danube River terrace that is covered by loess. Using luminescence dating, litho- and pedo-stratigraphy, and weathering proxies, we conclude that the fluvial section formed during Marine Isotope Stage (MIS) 6, and the overlying loess spans semi-continuously from late MIS 6 to the present. In order to use only elemental ratios unaffected by weathering and grain-size sorting, and thus serving as reliable provenance proxies, we introduce a novel statistical parameter – the path adherence coefficient (PAC). Along with the PAC, we also employ the well-established R^2 on geochemical data from the fluvial sediments. We identified Zr/Al_2O_3 and TiO_2/Al_2O_3 ratios as the most reliable provenance proxies, enabling us to discern temporal variations in sediment provenance at the Velika Vrbica LPS. The fine-grained portions of the LPS exhibit a significantly different provenance than that of the Danube River sediments. This difference is attributed to the transport of fine, loessial material over long distances, incorporating multiple sediment sources (likely originating from the Carpathians), from beyond the Danube River alluvium, into the loess. In contrast, the coarser, sand-rich sediment within the Velika Vrbica LPS section, which formed during MIS 2, has a more local provenance, having been derived almost exclusively from Danube River alluvium.

1. Introduction

Loess deposits are widely present across the Danube Basin and hold some of the longest terrestrial paleoenvironmental and paleoclimatic records in Europe, extending over the last million years (Smalley and Leach, 1978; Marković et al., 2011, 2015; Fitzsimmons et al., 2012). Their high accumulation rate enables paleoclimate and paleoenvironmental signals to be identified and analyzed at high resolution levels (Stevens et al., 2008; Perić et al., 2019). The geochemical composition of this loess and its intercalated paleosols is often used to reconstruct paleoweathering intensity, which is a proxy for paleotemperature and paleohumidity (Sheldon and Tabor, 2009; Schatz et al., 2014;

This article is part of a special issue entitled: PROTAGONIST published in Quaternary International.

* Corresponding author.
E-mail address: zoran.peric@geol.lu.se (Z.M. Perić).

https://doi.org/10.1016/j.quaint.2025.109969
Received 8 April 2025; Received in revised form 31 July 2025; Accepted 1 September 2025
Available online 8 September 2025

Campodonico et al., 2019). The chemical composition of Danubian loess has shown to provide excellent data on these types of paleoclimatic and paleoenvironmental dynamics (Buggle et al., 2008, 2011; Schatz et al., 2014; Újvári et al., 2014).

One of the main ways that loess, silt and dust form is via glacial grinding and weathering processes in cold, often glacial environments (Smalley, 1966; Mahaney and Andres, 1991; Bullard, 2013). Alternatively, processes such as salt weathering, eolian abrasion and fluvial comminution (which are also present in warmer climates) are also capable of producing silt particles (Pye and Sperling, 1983; Smith et al., 2002; Soreghan et al., 2016; Bristow and Moller, 2018), although not as effectively as do glacial processes. Loess forms when silt particles are entrained by wind, transported to downwind sites, and deposited (Pye, 1995; Smalley et al., 2009). The location/area from which silt is entrained is referred to as its provenance. However, loess provenance and even the mechanism(s) of loess formation are still a focus of research and debate (Stevens et al., 2013; Fenn et al., 2022), as there is a lack of consensus regarding the role of initial vs later/temporary sediment storage areas, the latter of which are represented by river terraces, floodplains or glacial deposits (Badura et al., 2013; Muhs, 2013). This impacts our understanding of sediment generation mechanisms and the role of eolian and fluvial sediment transport systems (Fenn et al., 2022, 2025). A better understanding of loess provenance could enhance our knowledge of paleowind strength and direction (Muhs and Budahn, 2006) and, consequently, improve our understanding of the entire atmospheric system (Fenn et al., 2022, 2025).

Smalley and Leach (1978) were the first to conduct a theoretical analysis on the provenance of Danubian loess. They argued that fluvial transportation of material plays a central role in loess formation, and that the eolian (transportation) stage is shorter-lasting and present across smaller distances. Many researchers have identified alluvium from the Danube River as the source of the Danubian loess (e.g. Buggle et al., 2008; Smalley et al., 2009; Újvári et al., 2012; Jipa, 2014; Marković et al., 2015). Geochemical analysis of Danubian loess, undertaken for the purpose of identifying its source(s), have shown that fluvial sediments and loess share similar geochemistry, and that the source material for loess has been, at least partly, recycled and homogenized prior to its final eolian accumulation (Buggle et al., 2008; Újvári et al., 2008). Investigation of the sedimentary pathways for Danubian loess in the lower Danube Basin (LDB, a term referring to the combined Wallachian (Dacian Basin) and Bulgarian Plain), based on chemical composition, showed that the Danube alluvium pathway is the most important loess source here. However, in the case of the northeastern LDB, transport pathways from the Carpathian Mountains appear to be important, especially in areas situated at a considerable distance from the Danube river itself (Pötter et al., 2021). The presence of local geochemical signatures of provenance was also demonstrated by Jordanova et al. (2024), who identified significant mafic contributions to loess in the Bulgarian Plain originating from Danube tributaries. Fenn et al. (2022) provide one of the most detailed studies of Danubian loess provenance, based on detrital zircon ages. Their study suggests that Danubian loess does not have a single source; instead, it may have been derived from various mountain ranges in the Danube Basin including the Swiss Alps, the Bohemian Massif, the Dinarides, the Carpathians and the Balkans. These results are important because they indicate that areas which were not extensively glaciated during the last glacial period, such as the Dinarides and the Carpathians, can still provide significant amounts of material for the formation of loess. The upshot of this is that glacial grinding and weathering processes in cold climate are not the only important ways that silt particles are formed (Fenn et al., 2022). The claims made in this paper were further solidified by Fenn et al. (2025), who identified Sahara dust contributions to Danubian loess as insignificant compared to material sourced from mountain ranges drained by the Danube and its tributaries, based on Sr–Nd isotopic data.

In short, the issue of loess provenence in the Danube Basin, which is home to such a deep loess record, is not yet settled. Thus, the objectives of this study are (1) to establish the geochemical sequence of the loess and the underlying fluvial sections situated at the westernmost part of the lower Danube Basin (Fig. 1A), (2) to compare the chemical composition of this loess and Danube alluvium, in order to determine the contributions of the Danube River to loess formation in the LDB, and (3) to identify potential provenance changes that occur in this LPS. We also conducted luminescence dating of the underlying fluvial section exposed at Velika Vrbica, so as to place the geochemistry and provenance results in their proper chronology.

2. Regional and local setting

Herein we use the term "multisection" to indicate the presence of two investigated sections located ~50 m from each other. The multisection is located in eastern Serbia, in the village of Velika Vrbica, next to the international border between Serbia and Romania and at a point where the Danube River exits the Iron Gate gorge and enters the LDB (Fig. 1A). The Iron Gate gorge system is carved perpendicularly across the Carpathian Mountains, connecting the middle and lower Danube basins. The geographical coordinates of the multisection are 44°35′1.7″N; 22°43′16″E, and the top of the multisection has an altitude of 78 m. The city of Kladovo is located 9 km to the west of the Velika Vrbica sections. Marović et al. (2007) indicate that the area has experienced vertical neoalpine subsidence, with displacements exceeding 2 km in places.

The area surrounding the profile is characterized by four terraces (Fig. 1C). These terraces are made up of predominantly fluvial gravel deposits (Bogdanović et al., 1980; Zeremski, 1972). All terraces, except Terrace 1, are covered by loess, which transitions into eolian sand toward the top. In contrast, Terrace 1 is directly overlain by eolian sand, with no intervening loess layer. Dune formations within the sand cover on Terraces 2, 3, and 4 characterize the area geomorphologically known as the "Kladovo Sand" (Zeremski, 1972). Wide transitional zones, which separate geomorphological units such as river terraces, are present as a consequence of this more recent eolian activity, which has overlaid terrace boundaries and made them more diffuse.

In terms of its local setting, the multisection is exposed along the sides of a gully incised into Terrace 3 of the Danube River, situated 28–30 m above the present-day river level (Fig. 1C). The gully is approximately 250 m long and cuts up to 17 m into loess, which overlies the fluvial terrace sediments, with only the uppermost part of the fluvial deposits exposed near the gully bottom. The gully terminates in a slopewash fan that extends toward the Danube River channel. Such gullies, predominantly formed in loess, are a common feature of loess terrains. They typically develop along the margins of loess plateaus or other elevated loess formations, primarily as a result of regressive erosion caused by precipitation draining from the plateau—or, in this case, from a river terrace (Leger, 1990).

3. Materials and methods

3.1. Optically stimulated luminescence (OSL) dating

Luminescence dating was performed on a 2.7-m thick fluvial section. The section was first cleaned back ~20 cm to uncover unweathered material; metal tubes (~5 cm diameter, 20 cm long) were then hammered into the freshly exposed section. A total of four samples were collected for OSL analysis, at depths of 1710 cm, 1740 cm, 1800 cm, and 1850 cm from the top of the Terrace 3. An additional 400 g of the surrounding sediment was also taken for environmental dose rate determination, and for field water content evaluation. All luminescence samples were prepared under subdued orange light at the Nordic Laboratory for Luminescence Dating (NLL) in Denmark, following the methodology suggested by Murray et al. (2021). The SAR protocols used for luminescence measurements, instrumentation and luminescence characteristics are all presented in Supplementary Information, as are details of the radionuclide concentrations (Table S1) and equivalent

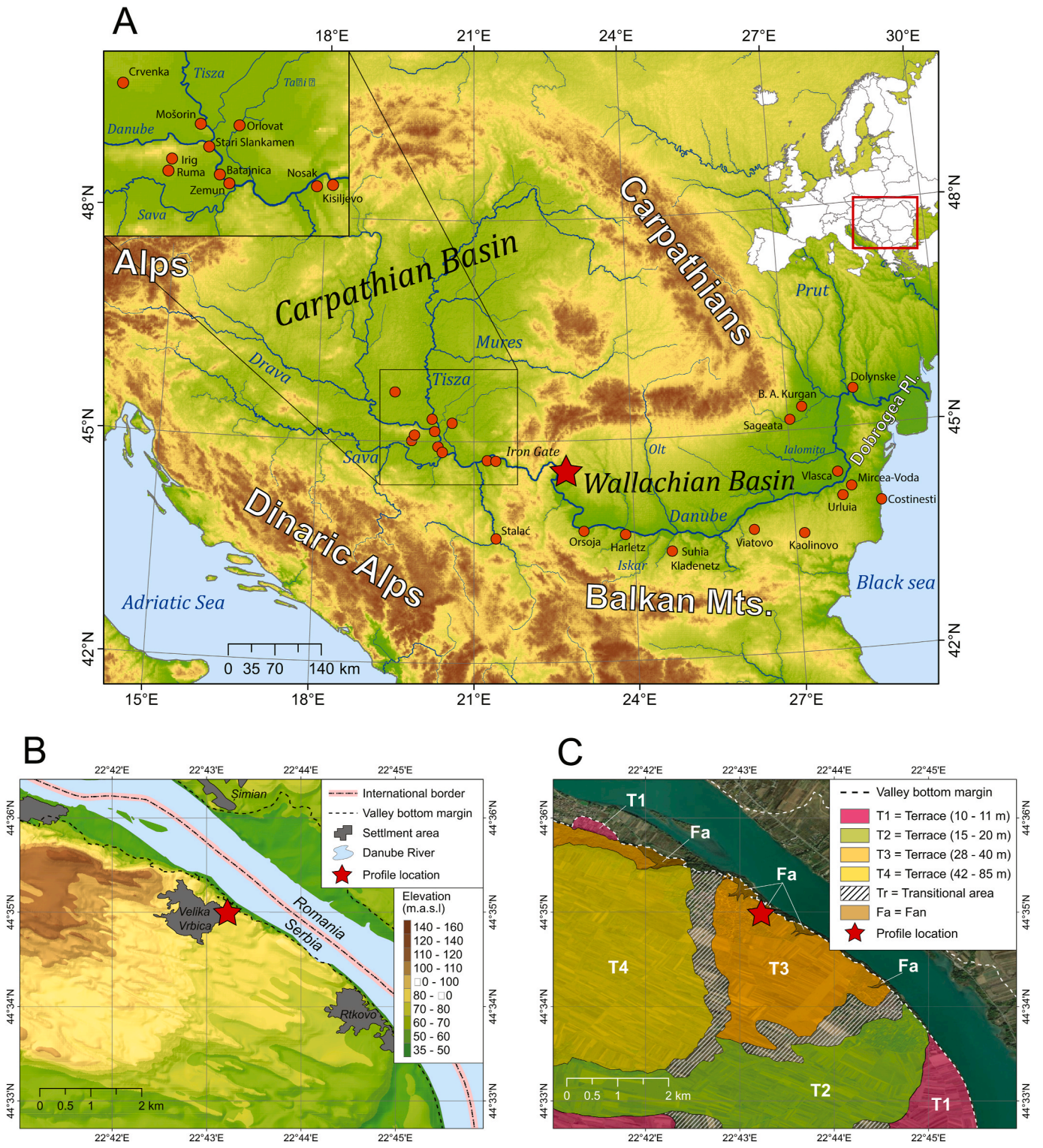

Fig. 1. A) Map of the middle and lower Danube Basin with the position of Velika Vrbica multisection (red star) and other LPSs identified with red circles (Avramov et al., 2006; Marković et al., 2014a, 2014b, 2015; Marković et al., 2014a, b, 2015; Obreht et al., 2015, 2017; Pötter et al., 2021; Laag et al., 2021; Perić et al., 2022; Jordanova et al., 2022a, 2022b); B) The setting of the Velika Vrbica multisection and C) A geomorphic map of the area surrounding the Velika Vrbica multisection (after Perić et al., 2025). (For interpretation of the references to color in this figure legend, the reader is referred to the Web version of this article.)

doses (Table S3). Luminescence ages for quartz and K-rich feldspar can be found summarised in Table 3.

3.2. Geochemical analyses

Prior to sampling, several centimeters of the surface layer was removed from the vertical profile to prevent contamination with freshly weathered, exposed sediment. Samples for geochemical analysis were collected at 5 cm intervals from the entire exposure at each of the two sites. Element concentrations by weight for Si, Al, Ca, Fe, K, Ti, Zn, Mn, Nb, Zr, Rb, and Sr were determined using a Thermo Fisher Scientific Niton XL2 XRF analyzer at the Laboratory for Paleoenvironmental

Reconstruction, Faculty of Sciences, University of Novi Sad. The XRF lacks the ability to measure the concentration of Na, and Mg concentrations are frequently below the detection limit. Therefore, these elements were not included in this study. Each sample was measured three times, and the average concentration value was used. Sample preparation involved hand grinding, air drying, and compression. Errors for Si, Al, Ca, Fe, K and Sr concentrations are $< \pm 5$ %, for Zr and Rb are $< \pm 10$ %, for Mn and Nb are $< \pm 15$ % and for Ti and Zn are $< \pm 25$ %. Error estimations are based on internal instrument error estimates. Afterward, the loss on ignition (LOI) was determined by heating the samples at 1000 °C for 8 h. The element concentrations were then LOI-normalized to eliminate biases introduced by varying amounts of organic matter, inorganic carbon, and humidity. The element concentrations for major elements (Si, Al, Ca, Fe, K, Ti and Mn) were converted to oxide form; trace elements were retained in elemental form. Due to differences in sample preparation and instrument calibration, the geochemical data obtained in this study are not directly comparable with other geochemical records and can only be used for comparisons within the same dataset.

In order to evaluate paleoclimatic and paleoenvironmental conditions during the loess-paleosol sequence formation, we employed two geochemical weathering indices. These indices rely on selective removal of mobile and soluble elements from a weathering profile, as compared to enrichment of immobile and weathering-resistant elements. Specifically, the weathering indices used in this study are in the form of a ratio where the concentration of immobile and weathering resistant element (Al_2O_3) serves as a numerator while concentration of mobile and soluble element (Sr, CaO) serves as denominator (Buggle et al., 2011). The use of elemental ratios enables us to overcome the dilution effect on element concentration.

We next conducted principal component analysis (PCA) on chemical composition data of both the loess and fluvial sediments. PCA is a statistical technique used for dimensionality reduction and has been used previously in loess research (Scull and Schaetzl, 2011). PCA identifies and prioritizes the most significant patterns (principal components) in a dataset (Jolliffe, 2002). To simplify interpretation, a varimax rotation was applied to the data, resulting in fewer elements with high loadings (correlations) for each component. The data was Z-normalized. The values of the two principal components (PC-1 and PC-2) with the highest total explained variance were utilized to generate a PCA plot.

In addition to the composition of the source terrain, other processes like weathering and grain-size sorting can influence the chemical composition of a sediment (Buggle et al., 2008; Xiong et al., 2010; Liang et al., 2013; Skurzyński et al., 2020), making the identification of provenance fingerprints less clear (Su et al., 2017). Here, we follow the approach of Fralick and Kronberg (1997), which has not yet been applied to loess provenance studies. This method is based on the analysis of element pairs. To appropriately reflect the provenance, the two elements need to be immobile, ensuring their ratio remains constant under changing weathering conditions. Additionally, the major mineral phases hosting those elements need to behave similarly during grain-size sorting. If both conditions are met, the ratio of those elements directly reflects the chemical composition of the source sediment and assumedly has not been influenced by weathering and grain-size sorting. Different values for these ratios are a signal of different sediment provenance (Fralick and Kronberg, 1997).

Scatterplots of major and trace elements in Fig. 5 are accompanied by mass gain–mass loss (MGML) paths. These paths extend from the origin along the line $y = ax$, indicating that the ratio between the two plotted elements (x and y) remains constant. This reflects a proportional increase or decrease in their concentrations. Element pairs which meet the two previously mentioned conditions will plot samples along MGML paths, where both elements will be proportionally enriched or depleted in certain grain size fractions. When this is the case, sediments with the same provenance consistently plot on the same MGML path. The movement of samples along different MGML paths is a clear indication of different origins (Fralick and Kronberg, 1997).

For this study, identification of element ratios suitable as provenance proxies relied on the chemical composition of Danube River alluvium, which is considered to have relatively constant provenance. We lack data on the chemical composition of other possible loess sources for the LDB, apart from Danube fluvial sediments. Consequently, we did not test whether element pairs for these other sediment sources plot along MGML paths. With that being said, if fluvial sediments follow the MGML path, the change in element ratio for loess samples could be linked to either a different source/provenance, or it could be attributed to the influence of weathering and grain-size sorting of other sources not known to us.

To identify element ratios suitable as indicators of loess provenance, we considered only element pairs for Al_2O_3, TiO_2, Zr and Nb, as these are relatively immobile elements (Bonjour and Dabard, 1991; Maynard, 1992; Nesbitt and Wilson, 1992; Nesbitt and Markovics, 1997; Young and Nesbitt, 1998) which tend to form insoluble hydrolysates during weathering (Buggle et al., 2011). To measure how closely fluvial samples follow the MGML path, we calculated sums of absolute residuals (SAR') for two linear regression models, one of which has the intercept term value set at zero, essentially representing the MGML path. Dividing the SAR' of the intercept-normalized model by the SAR' of the standard linear regression yields a coefficient, which we term the "path adherence coefficient" (PAC). A PAC_f (where "f" stands for fluvial) value of one indicates that fluvial samples perfectly follow the MGML path. For each element pair, we obtained two PAC_f values, with each element serving as both the x-axis and y-axis in the system. In the results section we displayed only lower PAC_f values for each element pair. The element ratios are constructed such that the element concentration used as the y-axis value is the numerator, while the element concentration serving as the x-axis value is the denominator. Additionally, the R^2 value for each standard linear regression was calculated. Statistical analyses were conducted using the R studio.

4. Results

4.1. Litho- and pedo-stratigraphy

The Velika Vrbica multisection comprises two distinct profiles: one characterized by eolian and the other by fluvial sediments (Fig. 2). The distance between the two profiles is ~50 m. The fluvial profile is located further down the gully; its uppermost surface is 5.5 m lower than the bottom of the loess section (Fig. 2A). Even though we have not observed the transition from fluvial to loessic sediments, the local geomorphology and the fact that both profiles are located on the same river terrace indicate that loess accumulated on top of fluvial sediments, i.e., fluvial deposition preceded eolian deposition.

The 2.7-m thick fluvial section consists of two types of adjoining sediments: on the one side fine to medium sandy material deposited by high energy channelized flow and on the other side silty/clayey sediments deposited by low energy (Table 1), overbank flow (Fig. 2B). The top of the fluvial section is strongly affected by bioturbation. The uppermost layer consists of 0.35 m of massive, silty, pale yellow, poorly developed paleosols. In the underlying 0.35 m, these paleosols alternate with tightly laminated sands containing rhizoliths. The next 0.40 m are again characterized by pale yellow, fine silty material. Notably, between depths of 1.10 and 1.20 m, agray-yellow sandy unit exhibits climbing ripple lamination. Beneath these climbing rippled sands, overbank gray-yellow fine silts are partly incised into fluvial sands through a small channel. Further down in the section there is a 0.55 m thick unit of gray, mostly non-laminated medium sands. Within this sandy unit, there are two layers present, each a few centimeters thick, that exhibit planar lamination and are more fine-grained than the rest of the unit. Below this sandy unit, there is a 0.7 m sequence of alternating non-laminated gray sands and massive fine silts/clays with signs of mottling. The base of the fluvial profile was not observed because it was not exposed

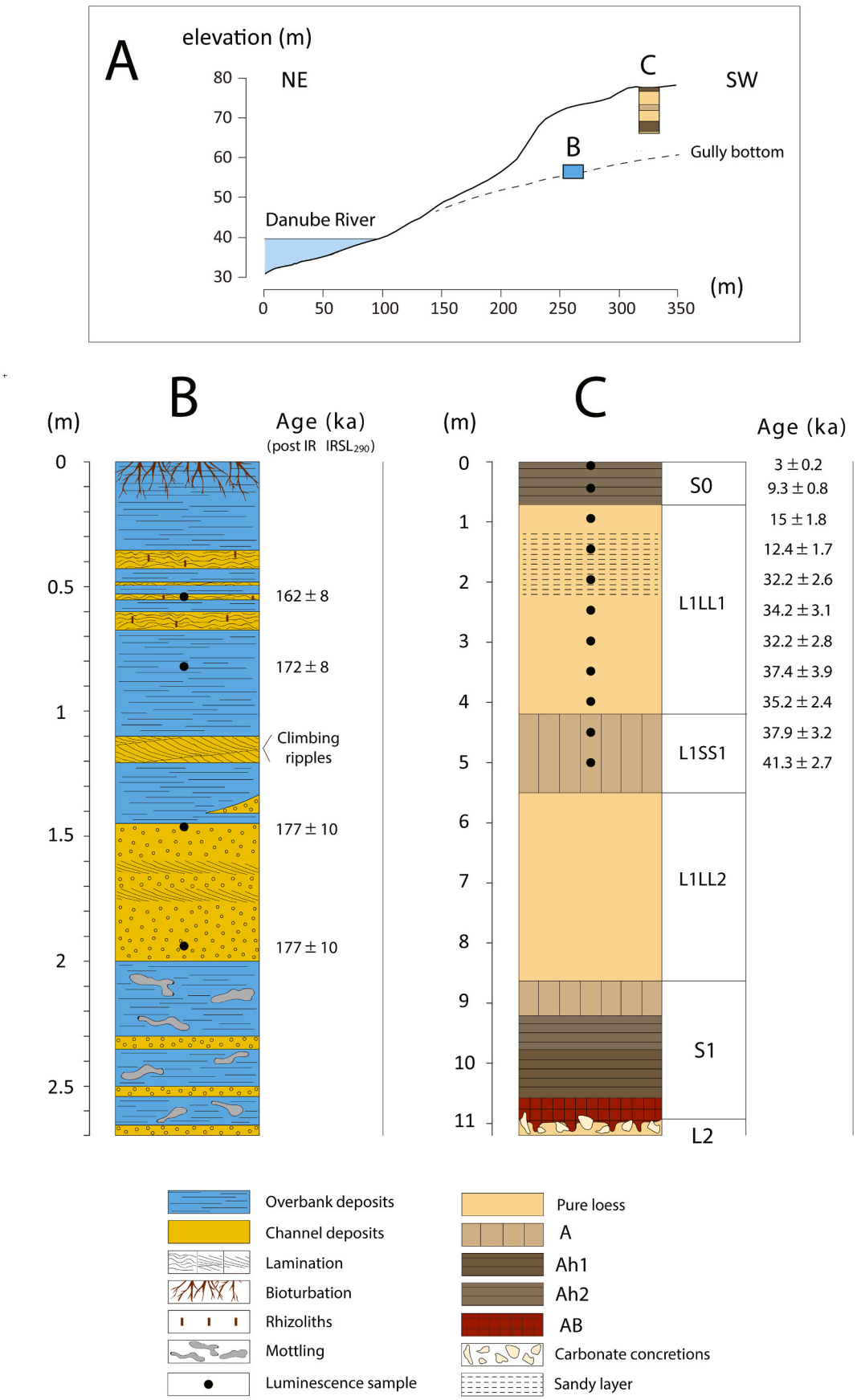

Fig. 2. A) Cross section of the Danube terrace at Velika Vrbica, exposed in the gully from NE to SW; B) Lithostratigraphic column of the fluvial section, accompanied by post IR $IRSL_{290}$ luminescence ages; and C) Litho- and pedo-stratigraphic column for the LPS accompanied by OSL luminescence ages, based on Perić et al. (2025). Note the difference in scale between the two logs.

Table 1
Lithological description of the Velika Vrbica fluvial section.

Unit	Thickness (cm)	Depth (cm)	Description
Ob and Ch deposits alteration	70	270–200	Alternating layers of massive, mostly gray fine silts/clays with signs of mottling and nonlaminated gray sands.
Channel deposits	55	200–145	Gray medium sands containing two layers of fine sands (few centimeters thick) which exhibit planar lamination.
Overbank deposits	25	145–120	Massive gray-yellow fine silts, partially incised into fluvial sands through a small channel.
Channel deposits	10	120–110	Fluvial sands, gray-yellow in color, with climbing ripple lamination.
Overbank deposits	110	110–70	Massive, pale yellow fine silts.
		70–35	Massive, silty, pale yellow, poorly developed paleosols which alternate with tighty laminated sands containg rhizolits.
		35–0	Massive, silty, pale yellow, poorly developed paleosols which are on the top strongly affected by bioturbation

within the gully.

The Velika Vrbica LPS has a total thickness of 11.2 m (Fig. 2C–Table 2). Here we use the Danube loess stratigraphic scheme proposed by Marković et al. (2015). Within the base of the profile, is the uppermost 30 cm of the L2 penultimate glacial loess unit, consisting of porous loess, rich in carbonate concretions and humic infiltrations. The boundary between the L2 loess and S1 pedocomplex above is significantly influenced by bioturbation. Considering the luminescence ages of the underlying fluvial sediments, which correspond to Marine Isotope Stage (MIS) 6 (refer to Section 3.2), along with the luminescence ages for the upper 5 m of the Velika Vrbica LPS (Perić et al., 2025), it is evident that the S1 unit, being the first observed pedocomplex from the top down, corresponds to the MIS 5 interglacial. This conclusion is further supported by the correlation between weathering index values and the benthic $\delta^{18}O$ records from LR04 (Lisiecki and Raymo, 2005), which represent a globally averaged deep-sea oxygen isotope stack compiled from benthic sediments at 57 marine sites worldwide, and are widely used as a proxy for global ice volume and paleoclimate (Fig. 3). The S1 pedocomplex has a thickness of 2.3 m, comprising four separate horizons. The lowermost reddish AB transitional horizon, with a weak angular blocky structure, spans from 10.90 m to 10.55 m. Above the AB horizon, Ah2 (darker, humic) and Ah1 (lighter, humic) horizons are developed, with a combined thickness of 1.35 m. Both are highly porous and have granular structure. The uppermost horizon of the S1 stratigraphic unit has the weakest developed soil. The A horizon of this soil extends from between 9.20 and 8.60 m depth, marking the gradual transition from interglacial to glacial conditions. Above the S1 pedocomplex there is 7.85 m of L1 loess that consists of three subunits: L1LL2, L1SS1 and L1LL1. The typical porous loess subunit, L1LL2, is present between 8.60 and 5.50 m. In the upper part of this subunit is a slightly darker, weakly developed A horizon of the L1SS1 subunit, measuring 1.30 m in thickness. Luminescence ages indicate that this subunit formed during MIS 3 (Perić et al., 2025). This interstadial paleosol with granular structure is covered by a 3.45 m thick L1LL1 loess subunit, predominantly composed of porous pale yellow and largely unaltered loess, which includes a 1.1 m thick unit of eolian sand in its upper part. The lowermost 1.5 m of this subunit, based on the age-depth model from Perić et al. (2025), formed during MIS 3, while the remainder of the subunit formed during MIS 2. Only the uppermost 10 cm of L1LL1 correspond to Holocene loess. The Holocene soil, S0, developed in the uppermost 75 cm of the investigated LPS.

Table 2
Lithological description of the Velika Vrbica LPS.

Unit	Thickness (cm)	Depth (cm)	Description
L2	30	1120–1090	Porous pale yellow loess with many carbonate concretions and humic infiltrations, intensively bioturbated.
S1	230	1090–1055	AB, slightly rubified, transitional horizon with weak angular blocky structure.
		1055–975	Ah1, darker humic horizon with granular structure.
		975–920	Ah2, lighter humic horizon with granular structure, weakly bioturbated.
		920–860	Initial weakly developed A horizon with granular structure.
L1	785	860–550	L1LL2 subunit, porous pale yellow loess.
		550–420	L1SS1 subunit, initial weakly developed A horizon with granular structure.
		420–225	L1LL1 subunit, porous pale yellow loess.
		225–115	L1LL1 subunit, eolian sand layer.
		115–75	L1LL1 subunit, sandy loess.
S0	75	75–0	Typical recent Ah2 humic horizon.

4.2. *Luminescence dating results for the fluvial section*

4.2.1. *Luminescence ages*

Table 3. Velika Vrbica quartz and K-rich feldspar luminescence ages presented with a comparison of the IR_{50}/OSL and $pIRIR_{290}$/OSL age ratios for evaluation of signal resetting in each sample.

4.2.2. *An assessment of potential age overestimation due to poor signal resetting*

While the luminescence chronology presented in Table 3 appears consistent with the stratigraphy it is not justifiable to assume that, on its own, this consistency means that the latent luminescence signal was fully reset prior to final deposition. The identification of incomplete signal resetting in sediments from fluvial settings remains an issue of great concern that has been well documented (Wallinga, 2002; Jain et al., 2004; Murray et al., 2012; Cunningham et al., 2015a, 2015b; Chamberlain and Wallinga, 2019; Ishii et al., 2022). In ancient fluvial settings it has even been established that poor/no signal resetting during transport prior to final deposition, can effectively be masked by what would appear to be whole sets of stratigraphically coherent luminescence ages (Utkina et al., 2022).

The potential threat of incomplete signal resetting and therefore significant age overestimation cannot be ignored and should be explicitly addressed in some way. It has been conclusively demonstrated that the post-IR IRSL (pIRIR) signals in K-rich feldspars bleach more slowly than the IR_{50} signal, and that the feldspar signals are reset more slowly than the quartz OSL signal (Poolton et al., 2002; Buylaert et al., 2012; Murray et al., 2012). Therefore, if the feldspar ages are consistent with the ages derived from the much easier to bleach quartz OSL, it is likely that the sample was fully reset at deposition (Møller and Murray, 2015). Using this comparative data to obtain ratios ($pIRIR_{290}$/OSL and IR_{50}/OSL) provides an effective and straightforward methodology for assessing signal resetting, and therefore the accuracy of the final ages (Alexanderson et al., 2024; Thompson et al., 2024; Schwendel et al., 2024). For our samples, these ratios are presented in Table 3, along with an assessment of signal resetting in the final column.

For sample vvf4 the $pIRIR_{290}$ and quartz OSL ages produce a ratio of 1.06 ± 0.37, which is within 10 % of unity. This suggests that the OSL and $pIRIR_{290}$ signals were fully bleached at the time of deposition. The IR_{50}/OSL ratio is well below unity (0.51 ± 0.18) for the sample, and even taking in to account anomalous fading of the feldspar signal (Lamothe and Auclair, 1999), any effect from this is likely to be much smaller than the residual dose that could be present due to incomplete bleaching (Murray et al., 2012). As such, the low IR_{50}/OSL ratio should

Table 3
Velika Vrbica quartz and K-rich feldspar luminescence ages presented with a comparison of the IR_{50}/OSL and $pIRIR_{290}$/OSL age ratios for evaluation of signal resetting in each sample.

Lab. code	Uncorrected age	Final age		Signal resetting		
	IR_{50}	POST IR $IRSL_{290}$	OSL	Age Ratio		Sufficiently well bleached
	(ka)	**(ka)**	(ka)	IR_{50}/OSL	pIRIR/OSL	
vvf1	73 ± 3	**162 ± 8**	79 ± 11	0.92 ± 0.13	**2.05 ± 0.29**	No
vvf2	78 ± 4	**172 ± 8**	131 ± 48	0.60 ± 0.22	**1.31 ± 0.48**	Yes
vvf3	77 ± 6	**177 ± 10**	145 ± 51	0.53 ± 0.19	**1.22 ± 0.44**	Yes
vvf4	85 ± 5	**177 ± 10**	166 ± 58	0.51 ± 0.18	**1.06 ± 0.37**	Yes

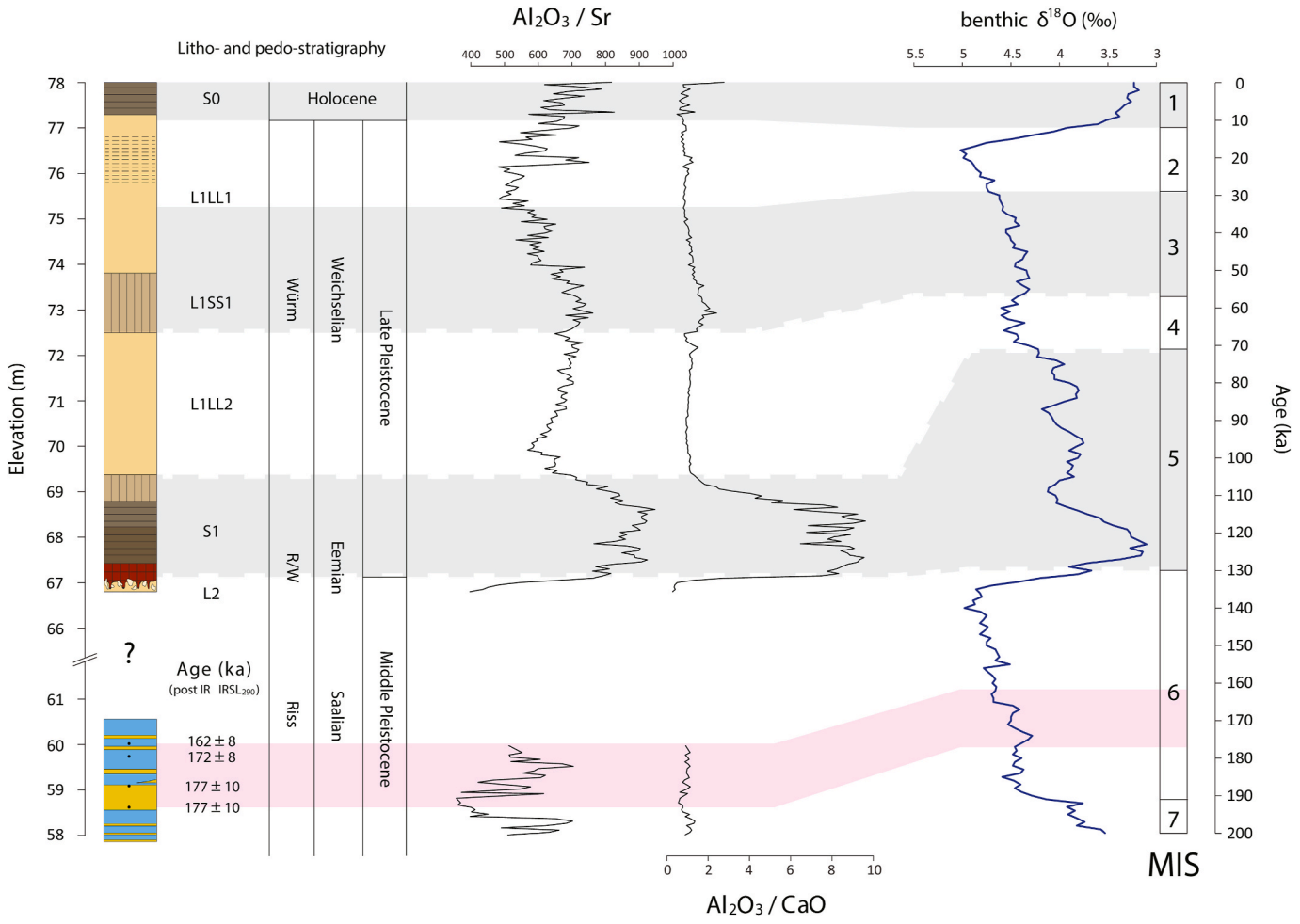

Fig. 3. Correlation between the Velika Vrbica loess and fluvial sections with the benthic $\delta^{18}O$ records from LR04 (Lisiecki and Raymo, 2005). Gray shading denotes correlations of the Velika Vrbica LPS with interglacial and interstadial periods, Dashed borders represent correlations of stratigraphic units with MIS-s, while non-dashed borders represent correlations based on the age-depth model from Perić et al. (2025) Pink shading represents the correlation for the fluvial section, based on obtained post IR $IRSL_{290}$ luminescence ages. (For interpretation of the references to color in this figure legend, the reader is referred to the Web version of this article.)

be interpreted as an additional indicator of complete signal resetting in sample vvf4. For samples vvf3 and vvf2 the $pIRIR_{290}$/OSL ratios are higher, but are still within 2 σ of unity, which is deemed acceptable in terms of good sample bleaching (Möller and Murray, 2015). Both samples also display a similarly low IR_{50}/OSL ratio, in common with vvf4. The $pIRIR_{290}$/OSL ratio of 2.05 ± 0.29, suggest vvf1 might not have been fully reset during its last transportation event. Taking into account the IR_{50}/OSL ratio appears to support this assertion. It is also considerably higher than the figure for the previous two samples, and almost twice that of vvf4 where we are certain that the sample was fully reset. However, while we should be cautious when interpreting the result for vvf1, its higher ratios may in fact be an artefact of the quartz being close to or above the 2D0 indicator of natural signal saturation, with the resulting OSL age significantly underestimating the true age of this sample.

In summary, the post-IR age results for vvf2, vvf3 and vvf4 are stratigraphically consistant with each other, and comparison of the pIRIR/OSL age ratios shows that they are also all within 2 σ of unity. This asserts that we can be confident that the $pIRIR_{290}$ signal in these samples was sufficiently reset prior to final deposition. In the case of vvf1 the $pIRIR_{290}$/OSL and IR_{50}/OSL age ratios suggests there could be a bleaching problem; however, the $pIRIR_{290}$ age is stratigraphically consistant and is statistically indistinguishable from the other 3 post-IR ages. Therefore, the higher ratios may simply be a result of signal

saturation in the quartz. If this is indeed the issue, then the $pIRIR_{290}$ age for vvf1 may actually also be valid. Our results show that the fluvial section formed during MIS 6, and furthermore, they confirm the MIS 5 age of the overlying S1 pedocomplex.

4.3. Geochemistry

Because LPSs can serve as a semi-continuous paleoclimate record, depth-variations in weathering, magnetic susceptibility, and grain size can provide insight into past climate and environmental conditions (Peng and Guo, 2001; Liang et al., 2013; Schatz et al., 2014; Újvári et al., 2014; Laag et al., 2021).

Stratigraphic interpretation of Fig. 3 is accompanied by values of two weathering indices (Al_2O_3/Sr and Al_2O_3/CaO). The L2 stratigraphic unit displays the lowest values for both weathering indices (Al_2O_3/Sr = 498; Al_2O_3/CaO = 0.53). In addition to indicating that this unit formed under glacial conditions, the low values for Al_2O_3/Sr and Al_2O_3/CaO near the top of the unit also result from carbonate precipitation during the formation of the S1 paleosol. (Finke and Hutson, 2008; Zhang et al., 2018). The S1 pedocomplex displays the highest degree of chemical alteration, suggestive of warm and humid interglacial conditions (Al_2O_3/Sr = 852; Al_2O_3/CaO = 6.71). The L1 loess displays low weathering indices values (Al_2O_3/Sr = 638; Al_2O_3/CaO = 1.12), which are characteristic of the cold and arid glacial period when soil development was minimal. Within the overall values of weathering indices for the L1 loess are low, the L1SS1 subunit exhibits somewhat higher values, correlated with the warmer MIS 3 interstadial (Al_2O_3/Sr = 703; Al_2O_3/CaO = 1.64). The weathering index values for the S0 soil suggest that it is not significantly weathered and is less weathered than the S1 pedocomplex. In fact, based on the Al_2O_3/Sr ratio, the S0 soil exhibits similar weathering to the initial soil formed during MIS 3, and it is even less weathered than that soil when considering the Al_2O_3/CaO ratio. However, it should be noted that the modern soil is strongly influenced by anthropogenic activity, especially agriculture and ploughing, which can alter the geochemical signal and lead to soil erosion (Skurzyński et al., 2020). The underlying fluvial section is less weathered than the Velika Vrbica LPS and exhibits Al_2O_3/CaO and Al_2O_3/Sr ratios similar to those of the least weathered loess.

Regarding the PCA (Fig. 4), principal components 1 and 2 (PC-1, PC-2) explained 66 % of data variance. PC-1, which explains a greater amount of variance (46 %), is strongly correlated with elements associated with the fine-grained fraction, e.g., Al_2O_3, Fe_2O_3, Rb, and K_2O (Table 4) (Liang et al., 2013; Liu et al., 2019; Li et al., 2020). Consequently, overbank fluvial sediments obtain the highest values on PC-1, while channel deposits and eolian sands have the lowest, with loess being positioned between (Fig. 4). This is further illustrated by the Al_2O_3-SiO_2 plot in Fig. 5, where fluvial and eolian sands exhibit the highest, while overbank deposits show the lowest SiO_2/Al_2O_3 ratio, reflecting differences in grain size (Peng and Guo, 2001; Liang et al., 2013). The negative correlation between these elements in the investigated samples indicates the dominance of quartz over aluminosilicates. However, when considering only loess and paleosol samples, a positive correlation emerges, highlighting the significant presence of feldspars, mica, and other aluminosilicates in loess. On the other hand, PC-2 values are not easily explained. The negative correlation with SiO_2 (Table 4) suggests that the sample's position on this axis reflects the amount of quartz present. However, negative correlations with Zr, TiO_2, and Nb (Table 4) suggest that additional processes are also at play. As will be

Table 4
PCA loading coefficients of analyzed chemical elements.

	loadings matrix	
	Principal component	
	1	**2**
Zr	0.48	0.64
Sr	0.36	−0.19
Rb	0.95	0.19
Zn	0.91	0.29
Fe_2O_3	0.94	0.3
MnO	0.76	0.13
TiO_2	0.37	0.69
Nb	0.18	0.69
CaO	−0.14	0.18
K_2O	0.93	0.18
Al_2O_3	0.95	0.08
SiO_2	−0.05	−0.84

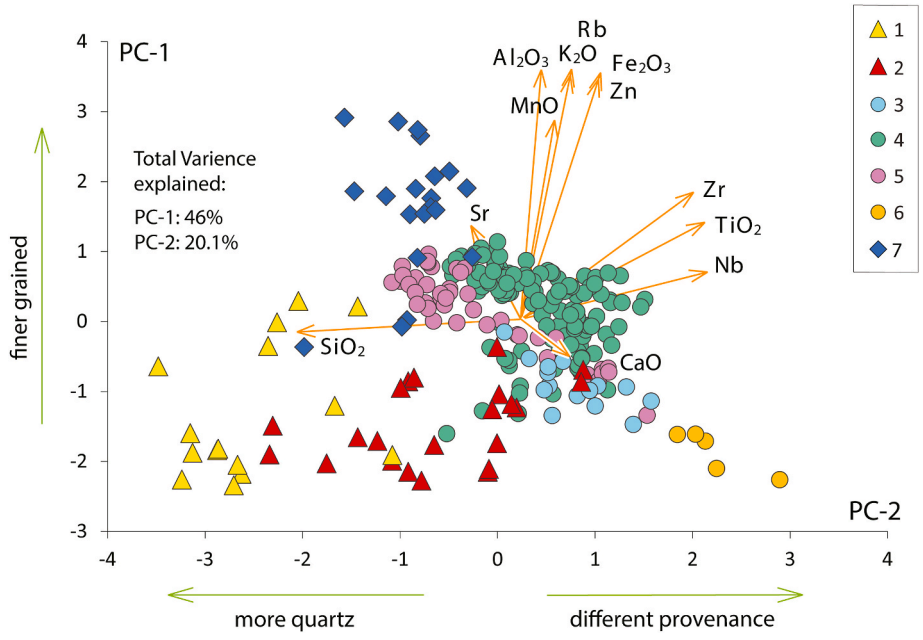

Fig. 4. Principal component diagram, applied to chemical composition of the loess and fluvial sediments. Orange arrows visualize the loadings matrix (Table 4). Legend: 1) channel deposits; 2) eolian sand; 3) S0 (recent soil); 4) L1 loess; 5) S1 pedocomplex; 6) L2 loess; 7) overbank fluvial deposits. (For interpretation of the references to color in this figure legend, the reader is referred to the Web version of this article.)

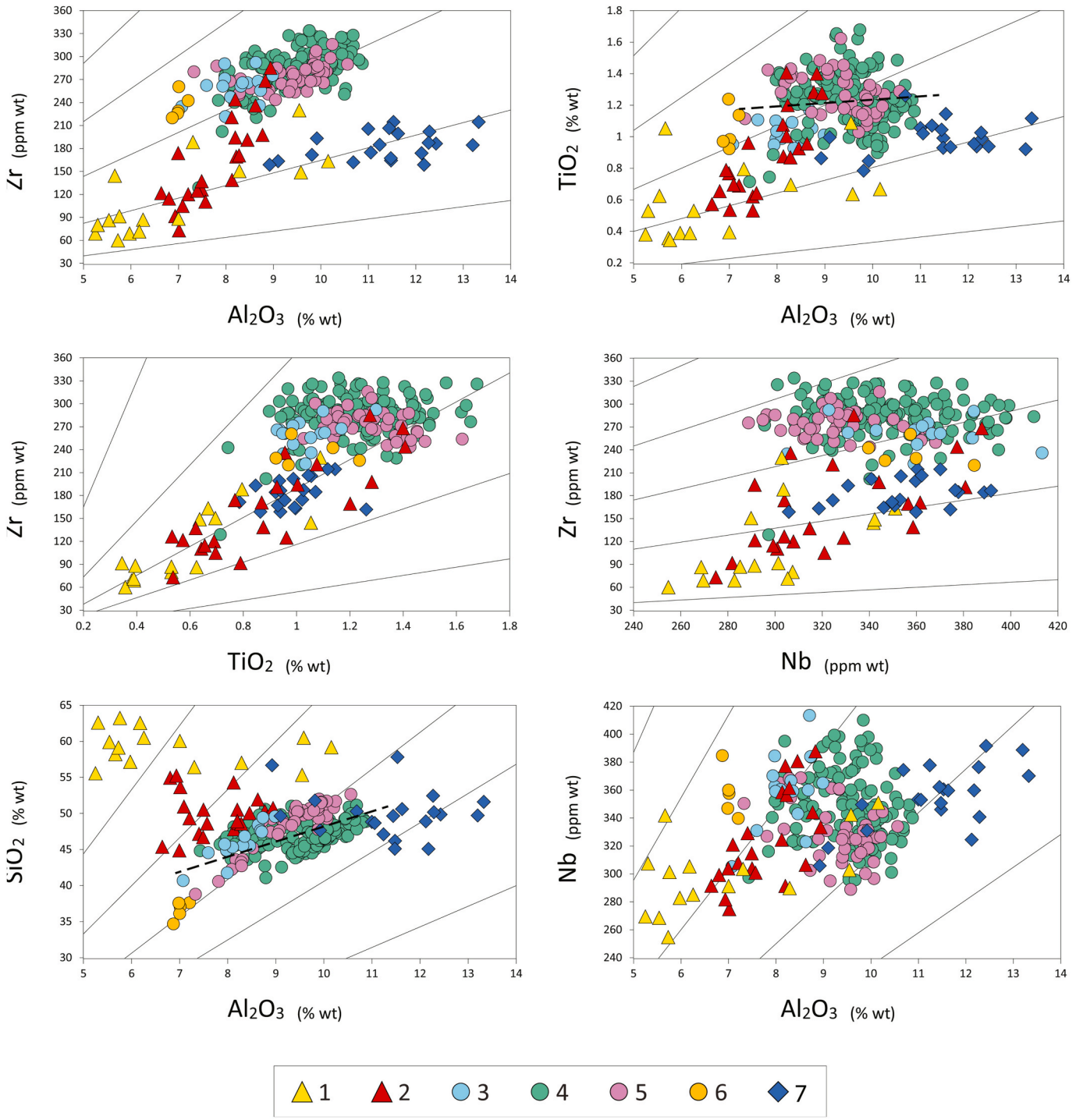

Fig. 5. Plots of major and trace element composition. Solid black lines represent MGML paths. Legend: 1) channel deposits; 2) eolian sand; 3) S0 (recent soil); 4) L1 loess; 5) S1 pedocomplex; 6) L2 loess; 7) overbank fluvial deposits. The dashed lines on Al_2O_3 - TiO_2 and Al_2O_3 - SiO_2 plots are linear trend lines for S0, L1, S1 and L2 samples.

shown later in the text, the differing provenance of fluvial versus eolian samples is responsible for variations in Zr and TiO_2 concentrations, with fluvial samples being depleted and eolian samples enriched in these elements. CaO is negatively correlated with PC-1 and positively correlated with PC-2. Although these correlations are not strong (Table 4), CaO primarily controls the distribution of L2 loess samples on the PCA plot (Fig. 4), as their CaO concentrations are more than double those of other loess units. As previously stated, L2 loess is strongly enriched in carbonates, partly because of leaching from the S1 paleosol, which caused precipitation of carbonates in the underlying loess (Finke and Hutson, 2008; Zhang et al., 2018).

We conclude that the greatest variability in the chemical composition of sediments is driven by grain size. However, provenance signatures are evident in the first two principal components when analyzing Danube fluvial and eolian sediments at Velika Vrbica.

Fig. 5 shows selected element pair scatterplots. The Al_2O_3–Zr plot is useful for discriminating between eolian and fluvial sediments, with both groups following their distinct MGML paths. This is evident from the PAC_f value of 0.99 and an R^2 value of 0.7 (Table 5). Fluvial sediments differentiate from eolian sediments in that the former are

Table 5
R^2 values for the standard linear regression model and PAC_f values fitted to fluvial sediments.

x	y	R^2	PAC_f
TiO_2	Zr	0.77	0.97
Al_2O_3	Zr	0.7	0.99
Al_2O_3	TiO_2	0.6	1.00
Nb	Zr	0.54	1.11
Nb	TiO_2	0.57	1.18
Nb	Al_2O_3	0.72	1.46

preferentially depleted in Zr. Interestingly, Zr concentration is higher in overbank deposits than in channel deposits, reflecting the dominance of fine-grained zircon minerals.

In addition to Zr, fluvial sediments are depleted in TiO_2. High variability in TiO_2 concentrations in loess may be partly attributed to higher analytical errors for TiO_2 content. It could also reflect different provenance, as TiO_2 has shown to be sensitive to provenance changes (Li, 2000), while it could also be attributed to the influence of grain-size sorting on other sources not investigated in this study. Despite a PAC_f value of 1.00, the low R^2 of 0.6 (Table 5) makes the TiO_2/Al_2O_3 ratio somewhat changeable for sediments with the same provenance. On the other hand, the TiO_2–Zr element pair has the highest R^2 value of 0.77, with a PAC_f value of 0.97, making it the most reliable provenance proxy. However, since eolian and fluvial sediments partially share the same MGML path (Fig. 5), their provenance, as indicated by the TiO_2/Zr ratio, is more similar than suggested by the previously mentioned ratios (Al_2O_3/Zr and TiO_2/Al_2O_3). Additionally, this ratio exhibits similar values for both fluvial and eolian sediments, making it less sensitive to capturing temporal provenance changes in loess and more easily affected by other factors, including grain-size sorting of sources other than Danube alluvium and analytical error.

The Nb content in the sediments appears to be influenced by grain-size sorting, as is evident from Al_2O_3–Nb plot. In this plot, the fluvial samples clearly deviate from the MGML paths (Fig. 5), with channel deposits showing enrichment and overbank deposits exhibiting depletion in Nb. As a result, element pairs involving Nb display the poorest results in terms of PAC_f values (Table 5), and therefore their ratios cannot be used as indicators of provenance.

5. Discussion

The PCA data (Fig. 4) suggest that the variability in the chemical composition of Velika Vrbica fluvial and eolian sediments is primarily driven by grain-size sorting effects (see Section 4.3). However, some variability also reflects differences in the provenance of loess and Danube fluvial sediments. Consequently, potential geochemical provenance fingerprints are partly masked by other processes. Nevertheless, we identified Zr/Al_2O_3 and TiO_2/Al_2O_3 ratios as useful provenance proxies which are not significantly influenced by other processes, based on analysis of the chemical composition of Danube sediment. Plotting these ratios against depth within the Velika Vrbica LPS allows us to discern provenance changes over time (Fig. 6). However, caution is needed when interpreting ratios involving Al_2O_3, especially subtle variations, as Al_2O_3 is mobile under extreme weathering/leaching conditions (Young and Nesbitt, 1998; Wang et al., 2023). The fact that Zr/Al_2O_3 and TiO_2/Al_2O_3 ratios do not show a systematic response to glacial–interglacial succession, such as consistently higher values during one period and lower during another (Fig. 6), suggests that these ratios are stable and thus reliable for temporal provenance analysis.

The Zr/Al_2O_3 and TiO_2/Al_2O_3 ratios for the Velika Vrbica LPS consistently plot along the margins of the fluvial sediment distribution (Fig. 6), indicating the influence of sources other than Danube alluvium. When examining the provenance of the L2 and S1 units, these ratios are not perfectly aligned. Zr/Al_2O_3 ratio indicates that L2 loess exhibits a more pronounced difference from fluvial sediments compared to the

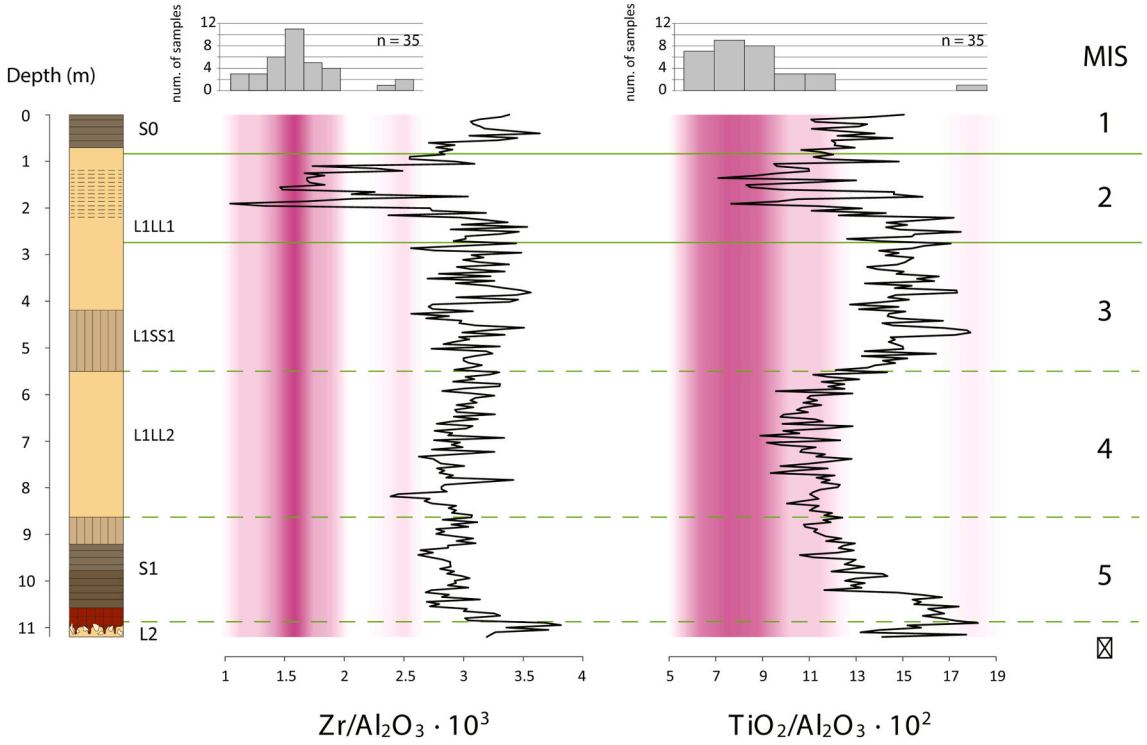

Fig. 6. Changes in provenance proxies with depth (black lines) at the Velika Vrbica LPS. Distribution plots at the top of the figure depict the distribution of provenance proxy values for fluvial sediments with "n" indicating the total number of samples. The pink shaded areas visualize this distribution, with the opacity of the color proportional to the frequency of values. Dashed green lines represent borders of stratigraphic units, while solid green lines represent MIS borders based on age-depth model from Perić et al. (2025). (For interpretation of the references to color in this figure legend, the reader is referred to the Web version of this article.)

lower part of the S1 pedocomplex, whereas the TiO_2/Al_2O_3 ratio suggests the opposite. This misalignment could be a consequence of Al_2O_3 weathering or grain-size sorting of sediment sources other than Danube alluvium. For most of the profile (upper 10.5 m), these ratios remain aligned, with their local maximum and minimum values appearing in the same stratigraphic units and subunits. Going from S1 to L1, loess provenance shifts more toward inputs of fluvial sediment, reaching its closest similarity to Danube sediment in the L1LL2 loess subunit, with both Zr/Al_2O_3 and TiO_2/Al_2O_3 values reaching their local maximum in different parts of the L1LL2. Moving from L1LL2 to L1SS1, the provenance once again shifts away from fluvial sediments, remaining stable in L1SS1. For TiO_2/Al_2O_3, this shift is more rapid and focused around the L1LL2 - L1SS1 stratigraphic transition. As L1LL2 can largely be correlated with MIS 4, the results suggest a higher input of local material derived from Danube alluvium during this period. This could be a consequence of drier and colder conditions, which limit vegetation growth and reduce stabilization of Danube alluvium. An increased presence of local material, indicated by sand beds and coarser grain size during MIS 4, has also been observed in many LPS of the Vojvodina region (Marković et al., 2008, 2023; Antoine et al., 2009; Vandenberghe et al., 2014).

The Zr/Al_2O_3 and TiO_2/Al_2O_3 values remain stable in the lower part of L1LL1 (Fig. 6), which, like L1SS1, correlates with MIS 3, based on luminescence data from Perić et al. (2025). A shift occurred during MIS 2, marked by the presence of an eolian sand layer. The sand has the most similar provenance to fluvial sediments, as indicated by both provenance proxies, but especially so in the Zr/Al_2O_3 ratio. Because eolian sand can only be transported short distances, this material is highly localized, predominantly originating directly from the Danube alluvium. In contrast, the remainder of the Velika Vrbica LPS is composed of finer dust particles (mostly silts) that can be transported across large distances, potentially representing a greater variety of source areas.

The presence of the sandy layer in the upper part of Velika Vrbica LPS could be a consequence of the regional climatic and environmental conditions, particularly when examined in the context of the nearby Poleva Cave site in south-western Romania. Poleva Cave is situated in the southern part of the Locvei Mountains, ~10 km north of the Danube Gorge and ~80 km east of the Velika Vrbica multisection. A stalagmite from this cave (PP10) offers a Late Pleistocene and Holocene isotopic record for this region (Constantin et al., 2007). This record indicates a growth hiatus between ~22 and 11 ka, which could correspond to a drier climatic interval, coinciding with conditions favorable for the intensification of eolian activity (Constantin et al., 2007). Several glacial advances have been documented in the southern Carpathians during the post-Last Glacial Maximum (LGM) phase (Urdea et al., 2023). Moreover, the geomorphology of the highest southwestern Carpathian massifs suggests that, during deglaciation, the glaciers remained positioned within the major relief landforms created by the LGM glaciers (Urdea et al., 2023). Therefore, the sedimentary interval represented by the eolian sand layer at the Velika Vrbica loess section can, most likely, be linked to an arid climatic event.

Just 20 cm below the Pleistocene-Holocene transition based on the age-depth model from Perić et al. (2025) occurs a sudden shift in provenance away from fluvial sources, as clearly indicated by both proxies (Fig. 6). This shift occurs just below the S0 recent soil and can be correlated with the transition to more humid interglacial (Holocene) climatic conditions. These conditions may have led to the stabilization of the Danube alluvium through increased vegetation cover, thereby reducing the availability of fluvial sands for eolian transportation.

The results not only indicate that the eolian sand layer within the Velika Vrbica LPS is of fluvial origin, but also suggest that Danube sediment has had a stable and consistent provenance since MIS 6, implying that sediment contributions from different parts of the Danube river catchment have not significantly changed between MIS 6 and MIS 2. Moreover, the transition from a fluvial to an eolian sedimentary environment occurred during MIS 6, with both the channel deposits and the L2 loess accumulating during this period. This indicates that the Danube rapidly abandoned Terrace 3 floodplain level, enabling eolian deposition over the underlying fluvial sediments.

The loess in the Velika Vrbica LPS exhibits higher concentrations of Zr and Ti than do the fluvial sediments below (Fig. 6). The difference in Zr concentration between the least and most Zr enriched loess sediments (excluding the eolian sands) is less than the difference in Zr concentration between fluvial and loess sediments (Fig. 6). This indicates that provenance influences Zr concentration more than weathering and grain size sorting, suggesting that Danube alluvium is not the sole source of loess in the Danubian basin and that there are significant differences in provenance between the loess of the Velika Vrbica LPS and Danube fluvial sediments. Previous studies (Jipa, 2014) have noted that loess sources from the Carpathians, including the catchments of the Olt, Vedea, and Ialomița rivers, contain higher concentrations of Zr than found in Danube alluvium. Pötter et al. (2021) reported significant sediment contributions from the Carpathians to the Sageata and Balta Alba Kurgan LPS in the NE of the LDB (Fig. 1), at considerable distances from the Danube alluvium. Consequently, the elevated Zr content in the Velika Vrbica loess could be attributed to sediment input from these sources. To further support this claim, a comparison of the chemical composition of sediments from the Danube and its tributaries draining the Balkan Mountains shows that only the Iskar River sediments (Fig. 1) have higher Zr concentrations than those of the Danube (Jordanova et al., 2024). This largely rules out the Balkan Mountains as a major source of the discrepancy in provenance between Danube sediments and loess at the Velika Vrbica. Although the Velika Vrbica LPS formed adjacent to the Danube, we suggest that its proximity to sediment production centers, particularly the Carpathians, may partly explain the significant input of material other than redeposited Danube sediments.

6. Conclusions

The Velika Vrbica LPS is located in the westernmost part of the LDB and has a record extending up to MIS 6. This LPS can be a valuable archive for understanding temporal changes in provenance due to its location and diverse sedimentary record. In this study, we provided an empirical framework for the method proposed by Fralick and Kronberg (1997), which helps us identify element ratios that can serve as provenance proxies. By calculating statistical parameters, including the novel parameter we propose (PAC) and the commonly used R^2, for Danube sediment samples, we identified Zr/Al_2O_3 and TiO_2/Al_2O_3 ratios as robust provenance proxies that are not significantly influenced by other processes, e.g., weathering and grain-size sorting.

The provenance context varies across different units of the Velika Vrbica LPS, with significant differences noted between loess and fluvial sediments. This difference can be attributed to the presence of other loess sources, apart from Danube alluvium (e.g., sources coming from the Carpathians), which are responsible for higher Zr and Ti contents in the Velika Vrbica loess compared to Danube fluvial sediments. The provenance of coarser sediments, such as eolian sands, is predominantly local, deriving almost solely from Danube River alluvium. In contrast, the provenance of finer-grained portions of the LPS is more complex, as long-distance transport enables the incorporation of multiple loess sources.

CRediT authorship contribution statement

Petar Krsmanović: Writing – original draft, Visualization, Software, Methodology, Investigation, Formal analysis, Conceptualization. **Zoran M. Perić:** Writing – review & editing, Writing – original draft, Project administration, Investigation, Funding acquisition, Formal analysis. **Warren Thompson:** Writing – review & editing, Writing – original draft, Investigation, Formal analysis. **Milica G. Radaković:** Writing – review & editing, Investigation, Formal analysis. **Cathal S. Ryan:** Writing – review & editing, Investigation. **Randall J. Schaetzl:** Writing

– review & editing. **Qingzhen Hao:** Writing – review & editing. **Tin Lukić:** Writing – review & editing. **Helena Alexanderson:** Writing – review & editing. **Slobodan B. Marković:** Supervision, Project administration, Investigation, Conceptualization.

Declaration of competing interest

The authors declare that they have no known competing financial interests or personal relationships that could have appeared to influence the work reported in this paper.

Acknowledgements

Zoran M. Perić is grateful to the Royal Physiographic Society in Lund (grants no. 42788 and 43046) for supporting his research on the age of loess in the Carpathian Basin. Slobodan B. Marković is grateful to the Silesian Technical University Professorship under the Excellence Initiative – Research University Programme for prominent researchers and Serbian Academy of Sciences and Arts grant F178. Milica Radaković expresses her gratitude for the support provided by the L'Oréal-UNESCO For Women in Science award. The authors acknowledge the support of the Provincial Secretariat for Higher Education and Scientific Research of Vojvodina (Serbia), No. 000871816 2024 09418 003 000 000 001 04 002 (GLOMERO), under Program 0201 and Program Activity 1012. We gratefully acknowledge Aleksa Krsmanović for his invaluable assistance in the development of the statistical parameter used in this study.

Appendix A. Supplementary data

Supplementary data to this article can be found online at https://doi.org/10.1016/j.quaint.2025.109969.

References

Alexanderson, H., Möller, P., Jain, M., Knudsen, M.F., Larsen, N.K., Perić, Z.M., Søndergaard, A.S., Thompson, W.K., 2024. Coupled luminescence and cosmogenic nuclide dating of postglacial deflation surfaces and sand drift on a raised ice-contact delta at Veinge, SW Sweden. Quat. Geochronol. 80, 101500. https://doi.org/10.1016/j.quageo.2024.101500.

Antoine, P., Rousseau, D.D., Fuchs, M., Hatté, C., Gauthier, C., Marković, S.B., Jovanović, M., Gaudenyi, T., Moine, O., Rossignol, J., 2009. High-resolution record of the last climatic cycle in the southern Carpathian Basin (Surduk, Vojvodina, Serbia). Quat. Int. 198, 19–36. https://doi.org/10.1016/j.quaint.2008.12.008.

Avramov, V.I., Jordanova, D., Hoffmann, V., Roesler, W., 2006. The role of dust source area and pedogenesis in three loess-palaeosol sections from North Bulgaria: a mineral magnetic study. Studia Geophys. Geod. 50, 259–282. https://doi.org/10.1007/s11200-006-0015-y.

Badura, J., Jary, Z., Smalley, I., 2013. Sources of loess material for deposits in Poland and parts of Central Europe: the lost Big River. Quat. Int. 296, 15–22. https://doi.org/10.1016/j.quaint.2012.06.019.

Bogdanović, P., Marković, V., Dragić, D., Dolić, D., Rakić, M., Babović, M., Rajčević, D., Popović, V., Milojević, Lj, 1980. Tumač Za Listove Donji Milanovac, Oršova, Baja De Arama i Turnu Severin (L 34-129, L 34-117, L 34-118, L 34-130): Osnovna Geološka Karta 1:100.000 [Explanatory Text to the Basic Geological Map 1:100,000]. Savezni Geološki Zavod.

Bonjour, J.L., Dabard, M.P., 1991. Ti/Nb ratios of clastic terrigenous sediments used as an indicator of provenance. Chem. Geol. 91, 257–267. https://doi.org/10.1016/0009-2541(91)90003-A.

Bristow, C.S., Moller, T.H., 2018. Testing the auto-abrasion hypothesis for dust production using diatomite dune sediments from the Bodélé depression in Chad. Sedimentology 65, 1322–1330. https://doi.org/10.1111/sed.12423.

Buggle, B., Glaser, B., Zöller, L., Hambach, U., Marković, S., Glaser, I., Gerasimenko, N., 2008. Geochemical characterization and origin of southeastern and eastern European loesses (Serbia, Romania, Ukraine). Quat. Sci. Rev. 27, 1058–1075. https://doi.org/10.1016/j.quascirev.2008.01.018.

Buggle, B., Glaser, B., Hambach, U., Gerasimenko, N., Marković, S., 2011. An evaluation of geochemical weathering indices in loess–paleosol studies. Quat. Int. 240, 12–21. https://doi.org/10.1016/j.quaint.2010.07.019.

Bullard, J.E., 2013. Contemporary glacigenic inputs to the dust cycle. Earth Surf. Process. Landf. 38, 71–89. https://doi.org/10.1002/esp.3315.

Buylaert, J.P., Jain, M., Murray, A.S., Thomsen, K.J., Thiel, C., Sohbati, R., 2012. A robust feldspar luminescence dating method for middle and Late Pleistocene sediments. Boreas 41, 435–451. https://doi.org/10.1111/j.1502-3885.2012.00248.x.

Campodonico, V.A., Rouzaut, S., Pasquini, A.I., 2019. Geochemistry of a Late Quaternary loess-paleosol sequence in central Argentina: implications for weathering, sedimentary recycling and provenance. Geoderma 351, 235–249. https://doi.org/10.1016/j.geoderma.2019.04.024.

Chamberlain, E.L., Wallinga, J., 2019. Seeking enlightenment of fluvial sediment pathways by optically stimulated luminescence signal bleaching of river sediments and deltaic deposits. Earth Surf. Dyn. 7, 723–736. https://doi.org/10.5194/esurf-7-723-2019.

Constantin, S., Bojar, A.V., Lauritzen, S.E., Lundberg, J., 2007. Holocene and Late Pleistocene climate in the sub-mediterranean continental environment: a speleothem record from Poleva Cave (Southern Carpathians, Romania). Palaeogeogr. Palaeoclimatol. Palaeoecol. 243, 322–338. https://doi.org/10.1016/j.palaeo.2006.08.001.

Cunningham, A.C., Evans, M., Knight, J., 2015a. Quantifying bleaching for zero-age fluvial sediment: a Bayesian approach. Radiat. Meas. 81, 55–61. https://doi.org/10.1016/j.radmeas.2015.04.007.

Cunningham, A.C., Wallinga, J., Hobo, N., Versendaal, A.J., Makaske, B., Middelkoop, H., 2015. Re-evaluating luminescence burial doses and bleaching of fluvial deposits using Bayesian computational statistics. Earth Surf. Dynam. 3, 55–65. https://doi.org/10.5194/esurf-3-55-2015.

Fenn, K., Millar, I.L., Durcan, J.A., Thomas, D.S., Banak, A., Marković, S.B., Veres, D., Stevens, T., 2022. The provenance of Danubian loess. Earth Sci. Rev. 226, 103920. https://doi.org/10.1016/j.earscirev.2022.103920.

Fenn, K., Millar, I.L., Bird, A., Veres, D., Wagner, D., 2025. Provenance of late Pleistocene loess in central and eastern Europe: isotopic evidence for dominant local sediment sources. Sci. Rep. 15, 1–15. https://doi.org/10.1038/s41598-024-83698-5.

Finke, P., Hutson, J.L., 2008. Modelling soil genesis in calcareous loess. Geoderma 145, 462–479. https://doi.org/10.1016/j.geoderma.2008.01.017.

Fitzsimmons, K.E., Marković, S.B., Hambach, U., 2012. Pleistocene environmental dynamics recorded in the loess of the middle and lower Danube basin. Quat. Sci. Rev. 41, 104–118. https://doi.org/10.1016/j.quascirev.2012.03.002.

Fralick, P.W., Kronberg, B.I., 1997. Geochemical discrimination of clastic sedimentary rock sources. Sediment. Geol. 113, 111–124. https://doi.org/10.1016/S0037-0738(97)00049-3.

Ishii, Y., Takahashi, T., Ito, K., 2022. Luminescence dating of cobbles from Pleistocene fluvial terrace deposits of the Ara River, Japan. Quat. Geochronol. 67, 101228.

Jain, M., Murray, A.S., Botter-Jensen, L., 2004. Optically stimulated luminescence dating: how significant is incomplete light exposure in fluvial environments? [Datation par luminescence stimulée optiquement: quelle signification en cas de blanchiment incomplet des sédiments fluviatiles?]. Quaternaire 15, 143–157.

Jipa, D.C., 2014. The conceptual sedimentary model of the Lower Danube loess basin: sedimentogenetic implications. Quat. Int. 351, 14–24. https://doi.org/10.1016/j.quaint.2013.06.008.

Jolliffe, I.T., 2002. Principal Components Analysis, second ed. Springer, Aberdeen.

Jordanova, D., Laag, C., Jordanova, N., Lagroix, F., Georgieva, B., Ishlyamski, D., Guyodo, Y., 2022a. A detailed magnetic record of Pleistocene climate and distal ash dispersal during the last 800 kyrs-the Suhia Kladenetz quarry loess-paleosol sequence near Pleven (Bulgaria). Global Planet. Change 214, 103840. https://doi.org/10.1016/j.gloplacha.2022.103840.

Jordanova, D., Simon, Q., Balescu, S., Jordanova, N., Ishlyamski, D., Georgieva, B., Bourles, D.L., Duvivier, A., Cornu, S., 2022b. Environmental changes in southeastern Europe over the last 450 ka: magnetic and pedologic study of a loess-paleosol profile from Kaolinovo (Bulgaria). Quat. Sci. Rev. 292, 107671. https://doi.org/10.1016/j.quascirev.2022.107671.

Jordanova, D., Jordanova, N., 2024. Geochemical and mineral magnetic footprints of provenance, weathering and pedogenesis of loess and paleosols from North Bulgaria. Catena 243, 108131. https://doi.org/10.1016/j.catena.2024.108131.

Laag, C., Hambach, U., Zeeden, C., Lagroix, F., Guyodo, Y., Veres, D., Jovanović, M., Marković, S.B., 2021. A detailed paleoclimate proxy record for the Middle Danube Basin over the last 430 kyr: a rock magnetic and colorimetric study of the Zemun loess-paleosol sequence. Front. Earth Sci. 9, 600086. https://doi.org/10.3389/feart.2021.600086.

Lamothe, M., Auclair, M., 1999. A solution to anomalous fading and age shortfalls in optical dating of feldspar minerals. Earth Planet Sci. Lett. 171, 319–323. https://doi.org/10.1016/S0012-821X(99)00180-6.

Leger, M., 1990. Loess landforms. Quat. Int. 7, 53–61. https://doi.org/10.1016/1040-6182(90)90038-6.

Liang, L., Sun, Y., Beets, C.J., Prins, M.A., Wu, F., Vandenberghe, J., 2013. Impacts of grain size sorting and chemical weathering on the geochemistry of Jingyuan loess in the northwestern Chinese Loess Plateau. J. Asian Earth Sci. 69, 177–184. https://doi.org/10.1016/j.jseaes.2012.12.015.

Li, X., Zan, J., Yang, R., Fang, X., Yang, S., 2020. Grain-size-dependent geochemical characteristics of Middle and Upper Pleistocene loess sequences from the Junggar Basin: implications for the provenance of Chinese eolian deposits. Palaeogeogr. Palaeoclimatol. Palaeoecol. 538, 109458. https://doi.org/10.1016/j.palaeo.2019.109458.

Li, Y.H., 2000. A Compendium of Geochemistry: from Solar Nebula to the Human Brain. Princeton Univ Press, Princeton.

Lisiecki, L.E., Raymo, M.E., 2005. A pliocene-pleistocene stack of 57 globally distributed benthic $\delta^{18}O$ records. Paleoceanography 20, 1003. https://doi.org/10.1029/2004PA001071.

Liu, D., Bertrand, S., Weltje, G.J., 2019. An empirical method to predict sediment grain size from inorganic geochemical measurements. G-cubed 20, 3690–3704. https://doi.org/10.1029/2018GC008154.

Marović, M., Toljić, M., Rundić, L., Milivojević, J., 2007. Neoalpine Tectonics of Serbia, first ed. Serbian Geological Society, Belgrade.

Marković, S.B., Bokhorst, M.P., Vandenberghe, J., McCoy, W.D., Oches, E.A., Hambach, U., Gaudenyi, T., Jovanović, M., Zöller, L., Stevens, T., Machalett, B.,

2008. Late Pleistocene loess-palaeosol sequences in the Vojvodina region, north Serbia. J. Quat. Sci. 23, 73–84. https://doi.org/10.1002/jqs.1124.
Marković, S.B., Hambach, U., Stevens, T., Kukla, G.J., Heller, F., McCoy, W.D., Oches, E. A., Buggle, B., Zöller, L., 2011. The last million years recorded at the Stari Slankamen (Northern Serbia) loess-palaeosol sequence: revised chronostratigraphy and long-term environmental trends. Quat. Sci. Rev. 30, 1142–1154. https://doi.org/10.1016/j.quascirev.2011.02.004.
Marković, S.B., Korać, M., Mrđić, N., Buylaert, J.P., Thiel, C., McLaren, S.J., Stevens, T., Tomić, N., Petić, N., Jovanović, M., Vasiljević, A. Dj, Sümegi, P., Gavrilov, B.G., Obreht, I., 2014a. Palaeoenvironment and geoconservation of mammoths from the Nosak loess–palaeosol sequence (Drmno, northeastern Serbia): initial results and perspectives. Quat. Int. 334, 30–39. https://doi.org/10.1016/j.quaint.2013.05.047.
Marković, S.B., Timar-Gabor, A., Stevens, T., Hambach, U., Popov, D., Tomić, N., Obreht, I., Jovanović, M., Lehmkuhl, F., Kels, H., Marković, R., Gavrilov, M.B., 2014b. Environmental dynamics and luminescence chronology from the Orlovat loess–palaeosol sequence (Vojvodina, northern Serbia). J. Quat. Sci. 29, 189–199. https://doi.org/10.1002/jqs.2693.
Marković, S.B., Stevens, T., Kukla, G.J., Hambach, U., Fitzsimmons, K.E., Gibbard, P., Buggle, B., Zech, M., Guo, Z., Hao, Q., Wu, H., O'Hara Dhand, K., Smalley, I.J., Újvári, G., Sümegi, P., Timar-Gabor, A., Veres, D., Sirocko, F., Vasiljević, Dj A., Jary, Z., Svensson, A., Jović, D., Lehmkuhl, F., Kovács, J., Svirčev, Z., 2015. Danube loess stratigraphy—Towards a Pan-European loess stratigraphic model. Earth Sci. Rev. 148, 228–258. https://doi.org/10.1016/j.earscirev.2015.06.005.
Marković, S.B., Vandenberghe, J., Perić, Z.M., Filyó, D., Bartyik, T., Radaković, M.G., Hao, Q., Marković, R.S., Lukić, T., Tomić, N., Gavrilov, M.B., Antić, A., Cvijanović, I., Sipos, G., 2023. Local differentiation in the Loess Deposition as a function of Dust source: key study Novo Orahovo Loess Paleosol sequence (Vojvodina, Serbia). Quaternary 6, 23. https://doi.org/10.3390/quat6010023.
Mahaney, W.C., Andres, W., 1991. Glacially crushed quartz grains in loess as indicators of long-distance transport from major European ice centers during the Pleistocene. Boreas 20, 231–239. https://doi.org/10.1111/j.1502-3885.1991.tb00153.x.
Maynard, J.B., 1992. Chemistry of modern soils as a guide to interpreting Precambrian paleosols. J. Geol. 100, 279–289. https://doi.org/10.1086/629632.
Möller, P., Murray, A.S., 2015. Drumlinised glaciofluvial and glaciolacustrine sediments on the Småland peneplain, South Sweden–new information on the growth and decay history of the Fennoscandian ice sheets during MIS 3. Quat. Sci. Rev. 122, 1–29. https://doi.org/10.1016/j.quascirev.2015.04.025.
Muhs, D.R., Budahn, J.R., 2006. Geochemical evidence for the origin of late Quaternary loess in central Alaska. Can. J. Earth Sci. 43, 323–337. https://doi.org/10.1139/e05-115.
Muhs, D.R., 2013. Loess and its geomorphic, stratigraphic, and paleoclimatic significance in the Quaternary. In: Shroder, J. F. (Editor-in-chief), Lancaster, N., Sherman, D.J., Baas, A.C.W. (Eds.), Treatise on Geomorphology, Vol 11, Aeolian Geomorphology. Academic Press, San Diego, pp. 149–183.
Murray, A.S., Thomsen, K.J., Masuda, N., Buylaert, J.P., Jain, M., 2012. Identifying well-bleached quartz using the different bleaching rates of quartz and feldspar luminescence signals. Radiat. Meas. 47, 688–695. https://doi.org/10.1016/j.radmeas.2012.05.006.
Murray, A., Arnold, L.J., Buylaert, J.P., Guérin, G., Qin, J., Singhvi, A.K., Smedley, R., Thomsen, K.J., 2021. Optically stimulated luminescence dating using quartz. Nat. Rev. Methods Primers 1, 72. https://insu.hal.science/insu-03418831.
Nesbitt, H.W., Wilson, R.E., 1992. Recent chemical weathering of basalts. Am. J. Sci. 292, 740–777. https://doi.org/10.2475/ajs.292.10.740.
Nesbitt, H.W., Markovics, G., 1997. Weathering of granodioritic crust, long-term storage of elements in weathering profiles, and petrogenesis of siliciclastic sediments. Geochem. Cosmochim. Acta 61, 1653–1670. https://doi.org/10.1016/S0016-7037(97)00031-8.
Obreht, I., Zeeden, C., Schulte, P., Hambach, U., Eckmeier, E., Timar-Gabor, A., Lehmkuhl, F., 2015. Aeolian dynamics at the Orlovat loess–paleosol sequence, northern Serbia, based on detailed textural and geochemical evidence. Aeolian Res. 18, 69–81. https://doi.org/10.1016/j.aeolia.2015.06.004.
Obreht, I., Hambach, U., Veres, D., Zeeden, C., Bösken, J., Stevens, T., Marković, S.B., Klasen, N., Brill, D., Burow, C., Lehmkuhl, F., 2017. Shift of large-scale atmospheric systems over Europe during late MIS 3 and implications for modern human dispersal. Sci. Rep. 7, 5848.
Peng, S., Guo, Z., 2001. Geochemical indicator of original eolian grain size and implications on winter monsoon evolution. Sci. China Earth Sci. 44, 261–266. https://doi.org/10.1007/BF02911995.
Perić, Z., Adolphi, E.L., Stevens, T., Újvári, G., Zeeden, C., Buylaert, J.P., Marković, S.B., Hambach, U., Fischer, P., Schmidt, C., Schulte, P., Huayu, L., Shuangwen, Y., Lehmkuhl, F., Obreht, I., Veres, D., Thiel, C., Frechen, M., Jain, M., Vött, A., Gavrilov, M.B., 2019. Quartz OSL dating of late quaternary Chinese and Serbian loess: a cross Eurasian comparison of dust mass accumulation rates. Quat. Int. 502, 30–44. https://doi.org/10.1016/j.quaint.2018.01.010.
Perić, Z.M., Marković, S.B., Avram, A., Timar-Gabor, A., Zeeden, C., Nett, J.J., Fischer, P., Fitzsimmons, K.E., Gavrilov, M.B., 2022. Initial quartz OSL and dust mass accumulation rate investigation of the Kisiljevo loess sequence in north-eastern Serbia. Quat. Int. 620, 13–23. https://doi.org/10.1016/j.quaint.2020.10.040.
Perić, Z.M., Ryan, C.S., Thompson, W., Radaković, M.G., Krsmanović, P., Alexanderson, H., Marković, S.B., 2025. Palaeoenvironmental changes recorded at the Velika Vrbica loess-palaeosol sequence, Wallachian Basin, during MIS 3–MIS 1. Boreas. https://doi.org/10.1111/bor.70009.
Poolton, N.R.J., Ozanyan, K.B., Wallinga, J., Murray, A.S., Bøtter-Jensen, L., 2002. Electrons in feldspar II: a consideration of the influence of conduction band-tail states on luminescence processes. Phys. Chem. Miner. 29, 217–225. https://doi.org/10.1007/s00269-001-0218-2.
Pötter, S., Veres, D., Baykal, Y., Nett, J.J., Schulte, P., Hambach, U., Lehmkuhl, F., 2021. Disentangling sedimentary pathways for the Pleniglacial lower danube loess based on geochemical signatures. Front. Earth Sci. 9, 600010. https://doi.org/10.3389/feart.2021.600010.
Pye, K., 1995. The nature, origin and accumulation of loess. Quat. Sci. Rev. 14, 653–667. https://doi.org/10.1016/0277-3791(95)00047-X.
Pye, K., Sperling, C.H.B., 1983. Experimental investigation of silt formation by static breakage processes: the effect of temperature, moisture and salt on quartz dune sand and granitic regolith. Sedimentology 30, 49–62. https://doi.org/10.1111/j.1365-3091.1983.tb00649.x.
Schatz, A.K., Scholten, T., Kühn, P., 2014. Paleoclimate and weathering of the Tokaj (NE Hungary) loess-paleosol sequence: a comparison of geochemical weathering indices and paleoclimate parameters. Clim. Past Discuss 10, 469–507. https://doi.org/10.5194/cpd-10-469-2014.
Scull, P., Schaetzl, R.J., 2011. Using PCA to characterize and differentiate the character of loess deposits in Wisconsin and Upper Michigan, USA. Geomorphology 127, 143–155. https://doi.org/10.1016/j.geomorph.2010.12.006.
Schwendel, A.C., Milan, D.J., Pope, R.J., Williams, R., Thompson, W.K., 2024. Using geophysical subsurface data for the reconstruction of valley-scale spatio-temporal floodplain evolution: implications for upland river restoration. Geomorphology 466, 339588. https://doi.org/10.1016/j.geomorph.2024.109459.
Sheldon, N.D., Tabor, N.J., 2009. Quantitative paleoenvironmental and paleoclimatic reconstruction using paleosols. Earth Sci. Rev. 95, 1–52. https://doi.org/10.1016/j.earscirev.2009.03.004.
Skurzyński, J., Jary, Z., Kenis, P., Kubik, R., Moska, P., Raczyk, J., Seul, C., 2020. Geochemistry and mineralogy of the Late Pleistocene loess-palaeosol sequence in Złota (near Sandomierz, Poland): implications for weathering, sedimentary recycling and provenance. Geoderma 375, 114459. https://doi.org/10.1016/j.geoderma.2020.114459.
Smith, B.J., Wright, J.S., Whalley, W.B., 2002. Sources of non-glacial, loess-size quartz silt and the origins of "desert loess". Earth Sci. Rev. 59, 1–26. https://doi.org/10.1016/S0012-8252(02)00066-1.
Smalley, I.J., 1966. The properties of glacial loess and the formation of loess deposits. J. Sediment. Res. 36, 669–676. https://doi.org/10.1306/74D7153C-2B21-11D7-8648000102C1865D.
Smalley, I.J., Leach, J.A., 1978. The origin and distribution of the loess in the Danube basin and associated regions of East-Central Europe – a review. Sediment. Geol. 21, 1–26. https://doi.org/10.1016/0037-0738(78)90031-3.
Smalley, I., O'Hara-Dhand, K., Wint, J., Machalett, B., Jary, Z., Jefferson, I., 2009. Rivers and loess: the significance of long river transportation in the complex event-sequence approach to loess deposit formation. Quat. Int. 198, 7–18. https://doi.org/10.1016/j.quaint.2008.06.009.
Soreghan, G.S., Joo, Y.J., Madden, M.E.E., Van Deventer, S.C., 2016. Silt production as a function of climate and lithology under simulated comminution. Quat. Int. 399, 218–227. https://doi.org/10.1016/j.quaint.2015.05.010.
Stevens, T., Carter, A., Watson, T.P., Vermeesch, P., Andò, S., Bird, A.F., Lu, H., Garzanti, E., Cottam, A.M., Sevastjanova, I., 2013. Genetic linkage between the Yellow River, the Mu Us desert and the Chinese Loess plateau. Quat. Sci. Rev. 78, 355–368. https://doi.org/10.1016/j.quascirev.2012.11.032.
Stevens, T., Lu, H., Thomas, D.S., Armitage, S.J., 2008. Optical dating of abrupt shifts in the late Pleistocene East Asian monsoon. Geology 36, 415–418. https://doi.org/10.1130/G24524A.1.
Su, N., Yang, S., Guo, Y., Yue, W., Wang, X., Yin, P., Huang, X., 2017. Revisit of rare earth element fractionation during chemical weathering and river sediment transport. G-cubed 18, 935–955. https://doi.org/10.1002/2016GC006659.
Thompson, W.K., Christensen, J., Murray, A.S., Autzen, M., 2024. Direct dating of an ancient stone causeway at Karlslunde, Sjælland, Denmark: a combined approach using luminescence from the surfaces of granitic cobbles and coarse grains from disaggregated heated rocks. Quat. Geochronol. 82, 101549. https://doi.org/10.1016/j.quageo.2024.101549.
Újvári, G., Varga, A., Balogh-Brunstad, Z., 2008. Origin, weathering, and geochemical composition of loess in southwestern Hungary. Quat. Res. 69, 421–437. https://doi.org/10.1016/j.yqres.2008.02.001.
Újvári, G., Varga, A., Ramos, F.C., Kovács, J., Németh, T., Stevens, T., 2012. Evaluating the use of clay mineralogy, Sr–Nd isotopes and zircon U–Pb ages in tracking dust provenance: an example from loess of the Carpathian Basin. Chem. Geol. 304, 83–96. https://doi.org/10.1016/j.chemgeo.2012.02.007.
Újvári, G., Varga, A., Raucsik, B., Kovács, J., 2014. The Paks loess-paleosol sequence: a record of chemical weathering and provenance for the last 800 ka in the mid-carpathian Basin. Quat. Int. 319, 22–37. https://doi.org/10.1016/j.quaint.2012.04.004.
Urdea, P., Ardelean, F., Ardelean, M., Onaca, A., 2023. The Romanian carpathians: glacial landforms during deglaciation (18.9–14.6 ka). In: Palacios, D., Hughes, P.D., García-Ruiz, J.M., Andrés, N. (Eds.), European Glacial Landscapes. Elsevier, pp. 165–173. https://doi.org/10.1016/B978-0-323-91899-2.00036-X.
Utkina, A.O., Panin, A.V., Kurbanov, R.N., Murray, A.S., 2022. Unexpectedly old luminescence ages as an indicator of the origin of the upper Volga River valley sediments. Quat. Geochronol. 73, 101381. https://doi.org/10.1016/j.quageo.2022.101381.
Vandenberghe, J., Marković, S.B., Jovanović, M., Hambach, U., 2014. Site-specific variability of loess and palaeosols (Ruma, Vojvodina, northern Serbia). Quat. Int. 334, 86–93. https://doi.org/10.1016/j.quaint.2013.10.036.
Wallinga, J., 2002. Optically stimulated luminescence dating of fluvial deposits: a review. Boreas 31, 303–322. https://doi.org/10.1111/j.1502-3885.2002.tb01076.x.

Wang, X., Algeo, T.J., Liu, W., Xu, Z., 2023. Effects of weathering and fluvial transport on detrital trace metals. Earth Sci. Rev., 104420 https://doi.org/10.1016/j.earscirev.2023.104420.

Xiong, S., Ding, Z., Zhu, Y., Zhou, R., Lu, H., 2010. Ã 6 Ma chemical weathering history, the grain size dependence of chemical weathering intensity, and its implications for provenance change of the Chinese loess–red clay deposit. Quat. Sci. Rev. 29, 1911–1922. https://doi.org/10.1016/j.quascirev.2010.04.009.

Young, G.M., Nesbitt, H.W., 1998. Processes controlling the distribution of Ti and Al in weathering profiles, siliciclastic sediments and sedimentary rocks. J. Sediment. Res. 68, 448–455. https://doi.org/10.2110/jsr.68.448.

Zhang, J., Li, S.H., Sun, J., Hao, Q., 2018. Fake age hiatus in a loess section revealed by OSL dating of calcrete nodules. J. Asian Earth Sci. 155, 139–145. https://doi.org/10.1016/j.jseaes.2017.11.016.

Zeremski, M., 1972. МорфодинаМика дунавских тераса у пределу Кључа [Morphodynamics of the Danube terraces in the Ključ area]. In: Зборник Радова Географског Института „Јован Цвијић, vol. 24.